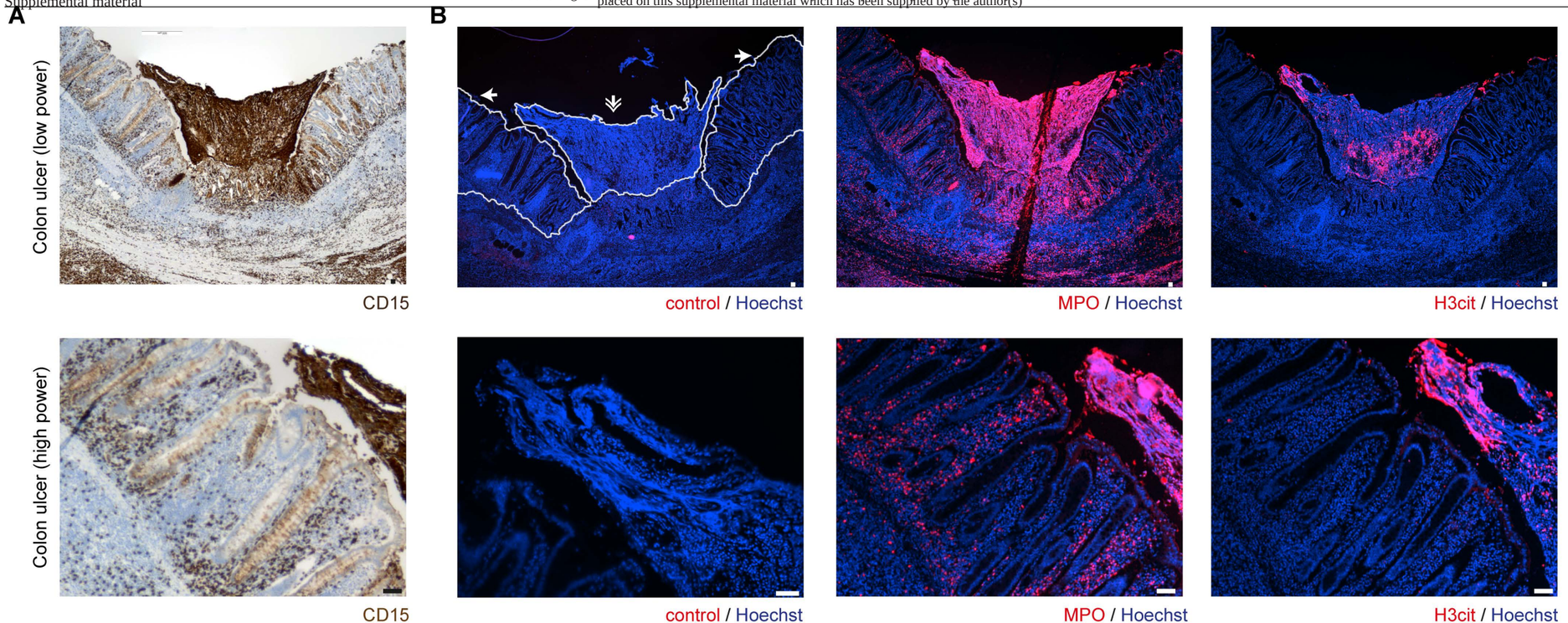

Supplementary Figure 1: Intercryptal lamina propria neutrophils mostly do not display PAD activity

(A) Low power (top) and high power (bottom) view of a human colon ulcer analysed for the presence of CD15 (DAB) and **(B)** myeloperoxidase (MPO), citrullinated histone H3 (H3cit) and. Note the broadly dispersed MPO in the fibrin layer, while MPO is also present in singly dispersed cells in the lamina propria. H3cit is strongly present in the fibrin layer whereas neutrophils in the intercryptal lamina propria are rather H3cit-negative. Please appreciate the decondensed chromatin in immunothrombi (scale bars = 100 µm) **(C)** Immunopositive cells in the intercryptal lamina propria as in (A–B) were quantified, displaying significantly less H3cit-positive cells in the intercryptal space, while MPO^+ and $CD15^+$ cells can be found in ample amounts (n = 10 samples, ** $p < 0.01$, Student's t-test).

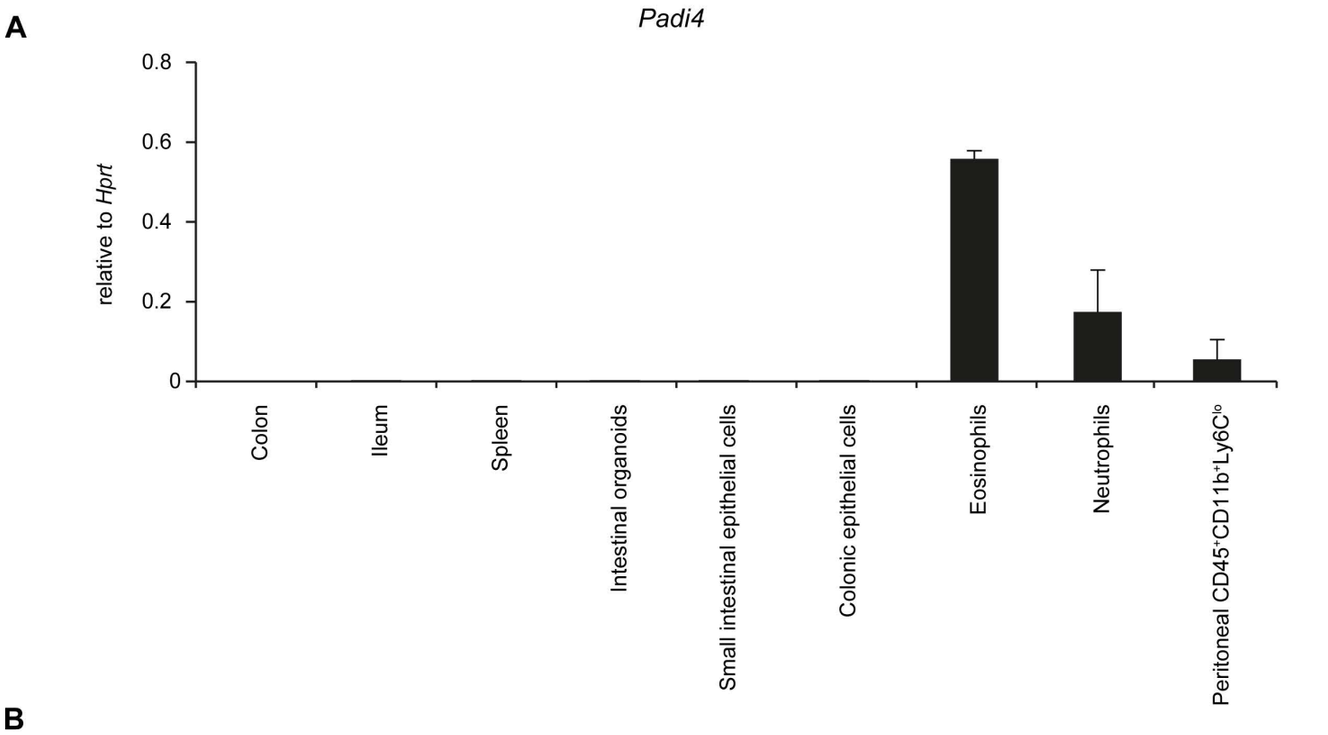
A
Padi4
relative to Hprt
0.8
0.6
0.4
0.2
0
Colon
Ileum
Spleen
Intestinal organoids
Small intestinal epithelial cells
Colonic epithelial cells
Eosinophils
Neutrophils
Peritoneal CD45+CD11b+Ly6Clo

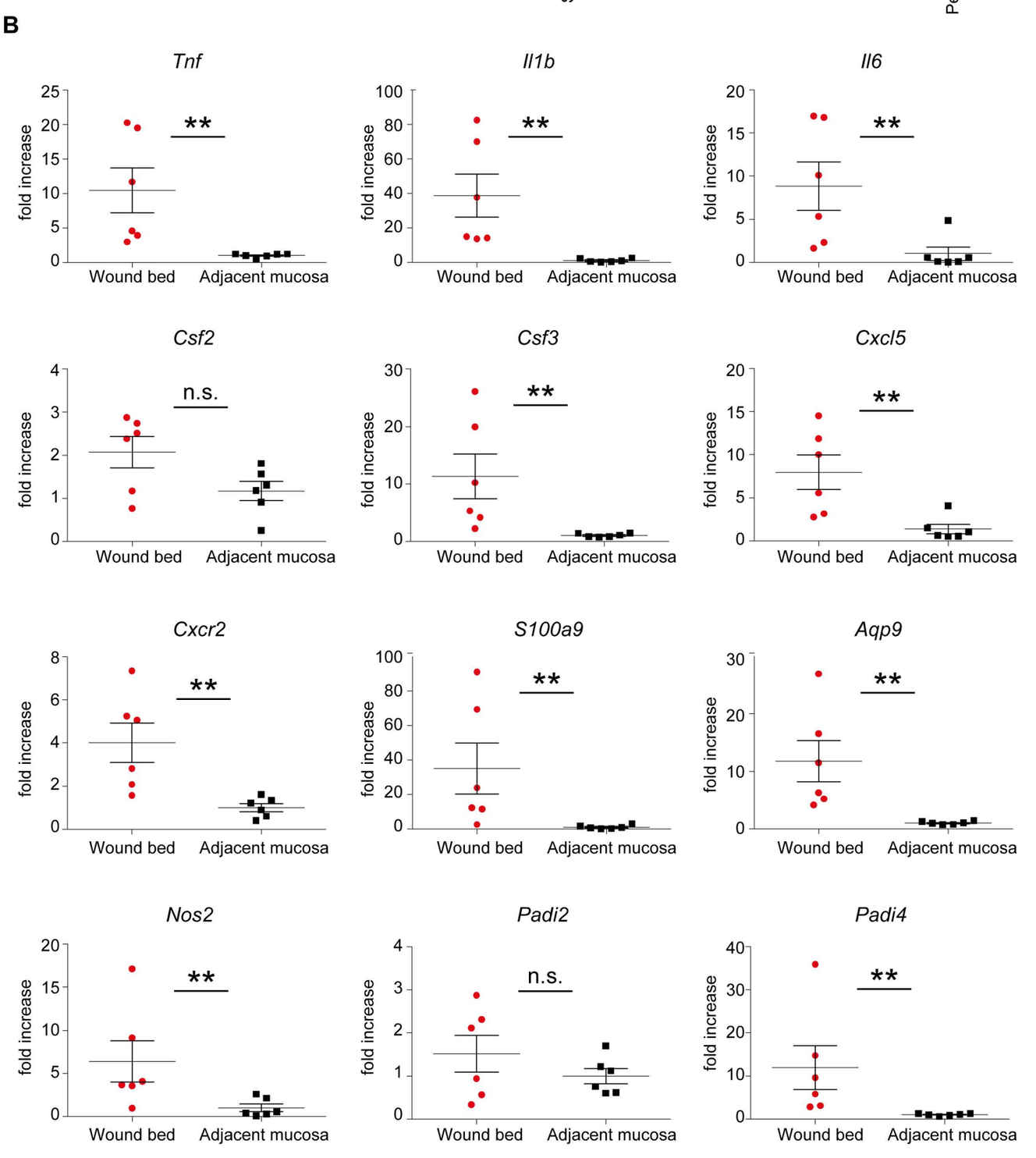
B
Tnf
Il1b
Il6
Csf2
Csf3
Cxcl5
Cxcr2
S100a9
Aqp9
Nos2
Padi2
Padi4
fold increase
Wound bed
Adjacent mucosa
**
n.s.

Supplementary Figure 2: *Padi4* is expressed in myeloid cells, predominantly granulocytes and is significantly increased in the colon wound bed

(A) RT-PCR analyses show a prevailing expression of *Padi4* in neutrophils and eosinophils and to a smaller extent in peritoneal Ly6C-low monocytes, whereas no expression of *Padi4* was detected in whole colon or ileum, isolated epithelial cells, spleen or intestinal organoids. **(B)** Analysis of mRNA expression of selected neutrophil- and inflammation-related genes in forceps-induced colonic wound beds and adjacent healthy mucosa was performed at 24 hours post-injury, displaying markedly increased abundance of neutrophil- and inflammation-related transcripts (at least n = 6 samples per group (** $p < 0.01$, Student's t-test, mean + SEM are depicted).

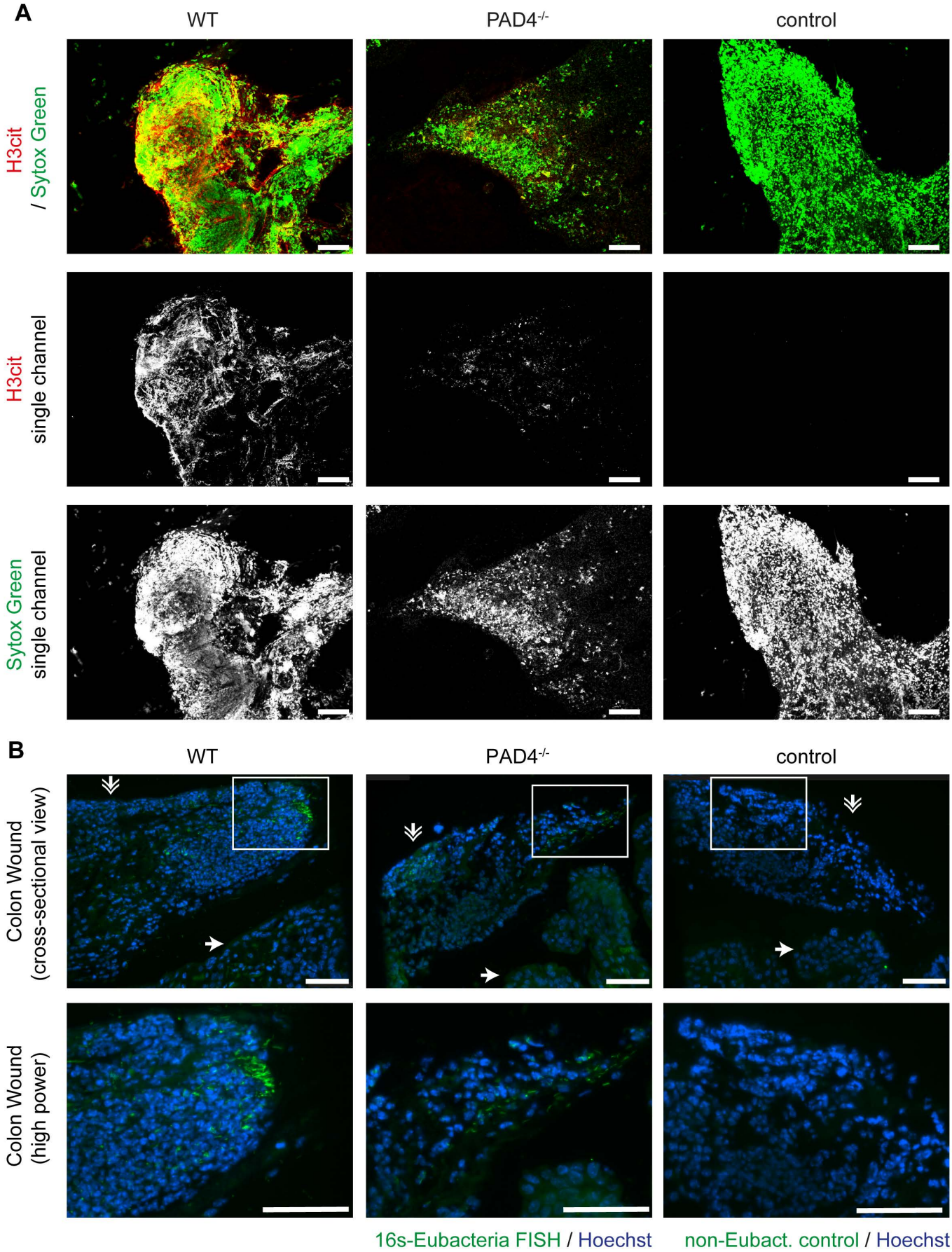
A
WT
PAD4-/-
control
H3cit / Sytox Green
H3cit single channel
Sytox Green single channel
B
WT
PAD4-/-
control
Colon Wound (cross-sectional view)
Colon Wound (high power)
16s-Eubacteria FISH / Hoechst
non-Eubact. control / Hoechst

Supplementary Figure 3: PAD4-deficient mice fail to adequately decondense neutrophil chromatin in immunothrombi on mucosal wounds

(A) Manually grasped immunothrombi from colon wounds were subjected to immunofluorescence. Decondensed chromatin is a striking feature in immunothrombi as evidenced by SYTOX Green staining. We detected H3cit throughout the immunothrombus, which is strongly diminished in fibrinoid derived from PAD4$^{-/-}$ mice. **(B)** Cross-sections of colon wounds were subjected to fluorescent *in-situ* hybridisation using 16S-rRNA-Eubacteria directed probes. The immunothrombi of both wild-type and PAD4$^{-/-}$ mice (indicated by the double-head arrow) was infiltrated by bacteria, while none were detected in deeper layers of the mucosa (the ulcer edge is highlighted by a single head arrow). Low power and high power magnification are presented. (Scale bars = 100 µm).

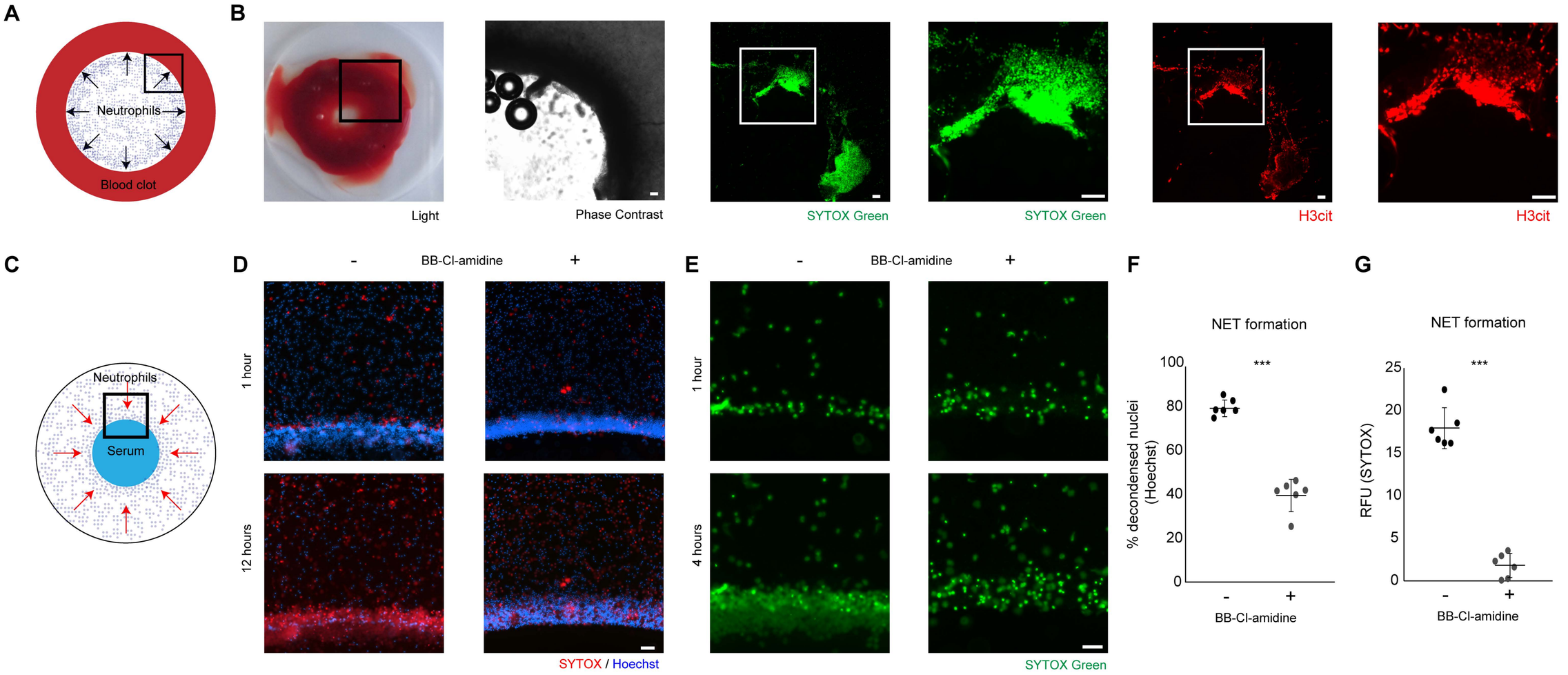

Supplementary Figure 4: PAD4-mediated NET formation is instigated in high cellular densities at the edge of a blood clot in the absence of bacteria

(A) Human citrated whole blood was clotted by recalcification. 2×10^5 isolated human neutrophils were cultured in autologous serum and added to the punched-out center of the clot (31 mm², scale bar = 2 mm). **(B)** This setup was analysed by brightfield (left) and immunofluorescence: Decondensed SYTOX Green$^+$ (center) and H3cit$^+$ chromatin (right) was preferentially formed at the edge of the blood clot as depicted in representative photomicrographs. Scale bars = 100 µm. **(C–G)** Human neutrophils were cultured in RPMI medium supplemented with 2 % autologous serum in the presence and absence of the pan-PAD inhibitor BB-Cl-amidine (20 µM) or solute control in a well prepared with an agarose gel in the center containing 20 % autologous serum. **(C)** A graphic model of this experimental setup is presented. The black box represents a typical field of view as presented in D, E. **(D)** The edge of the surrogate clot is presented at two different time points after stimulation in the presence and absence of the PAD inhibitor BB-Cl-amidine. Hoechst shows all nucleated cells in blue, while SYTOX Green staining of extracellular DNA and permeable cells is depicted in red, representative images of three independent experiments. Please appreciate the increased presence of condensed chromatin at the edge of the clot in the presence of the pan-PAD inhibitor, whereas more chromatin is decondensed in its absence. Scale bars = 100 µm. **(E)** The SYTOX Green channel of this experimental setup is displayed after 1 and 4 hours. Please appreciate the strongly reduced chromatin decondensation at the edge of the clot in the presence of BB-Cl-amidine. Scale bars = 100 µm. **(F)** NET formation was quantified in images as depicted in (D, E) by quantification of decondensed nuclei at the clot edge using the Hoechst signal and **(G)** by use of fluorescence intensity quantification of the SYTOX signal (*** $p < 0.001$, Student's t-test, three independent experiments reported). Scale bars = 100 µm.

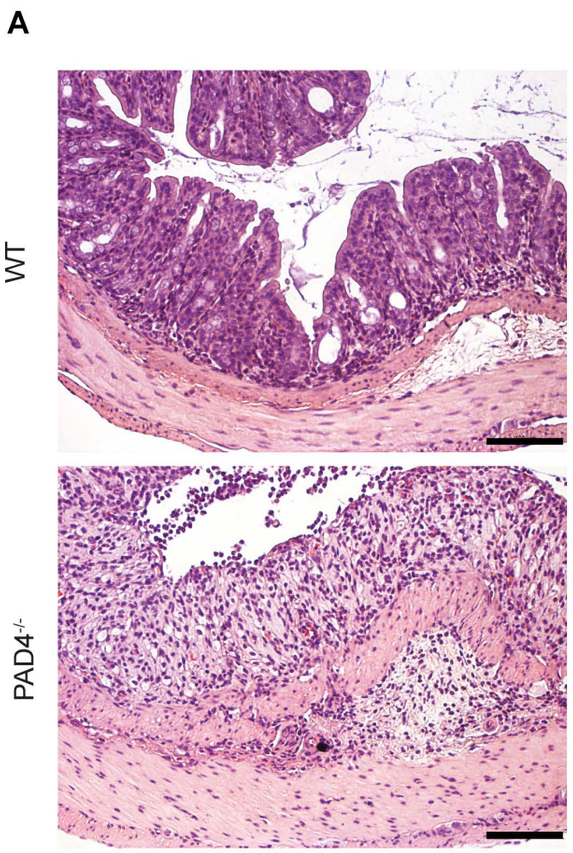
A
WT
PAD4-/-
H&E

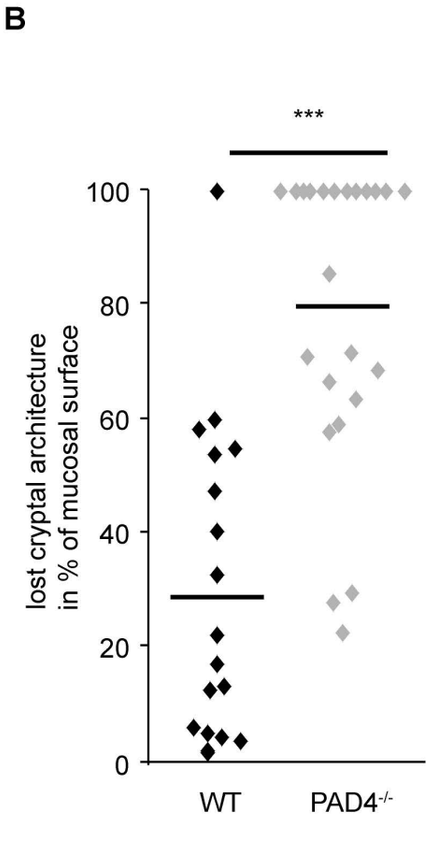
B
***
lost cryptal architecture in % of mucosal surface
100
80
60
40
20
0
WT
PAD4-/-

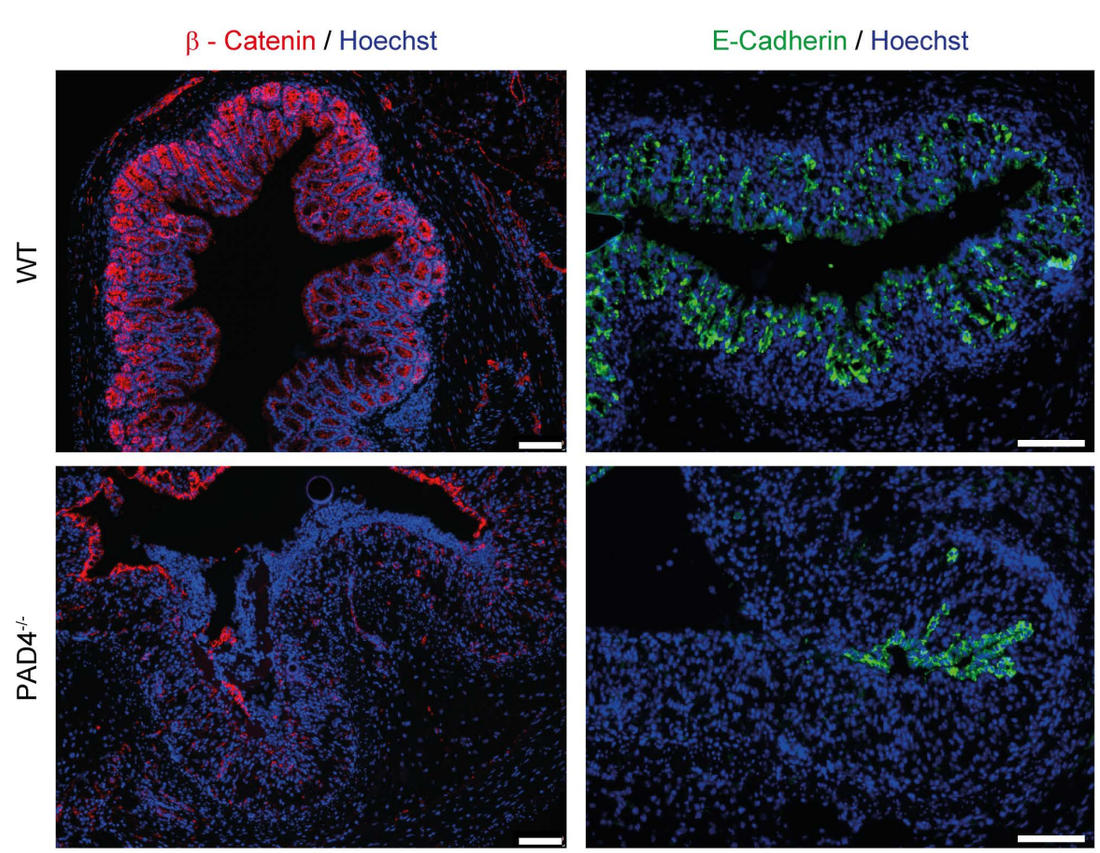
C
β - Catenin / Hoechst
E-Cadherin / Hoechst
WT
PAD4-/-

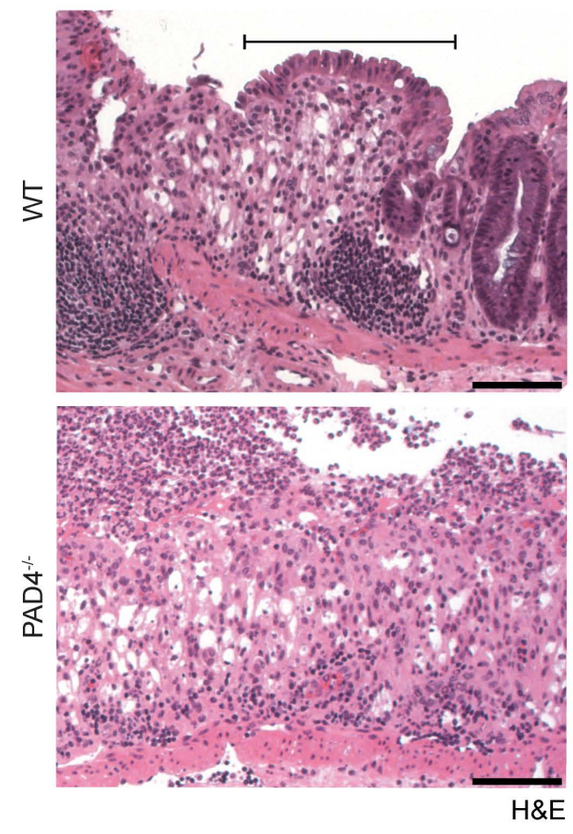
D
WT
PAD4-/-
H&E

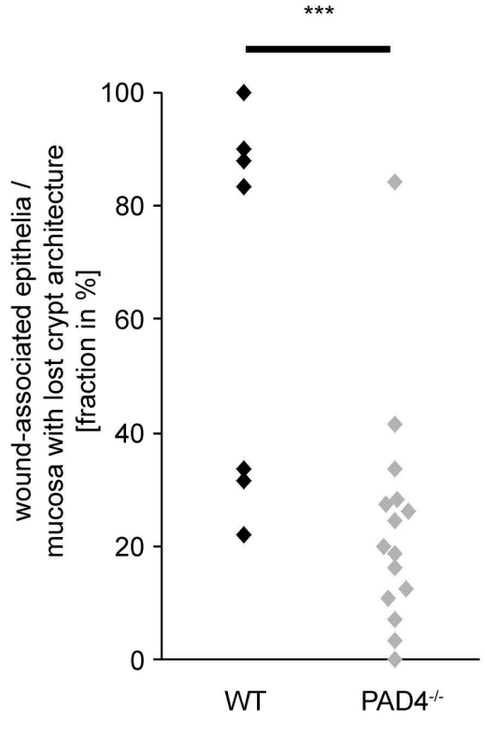
E
***
wound-associated epithelia / mucosa with lost crypt architecture [fraction in %]
100
80
60
40
20
0
WT
PAD4-/-

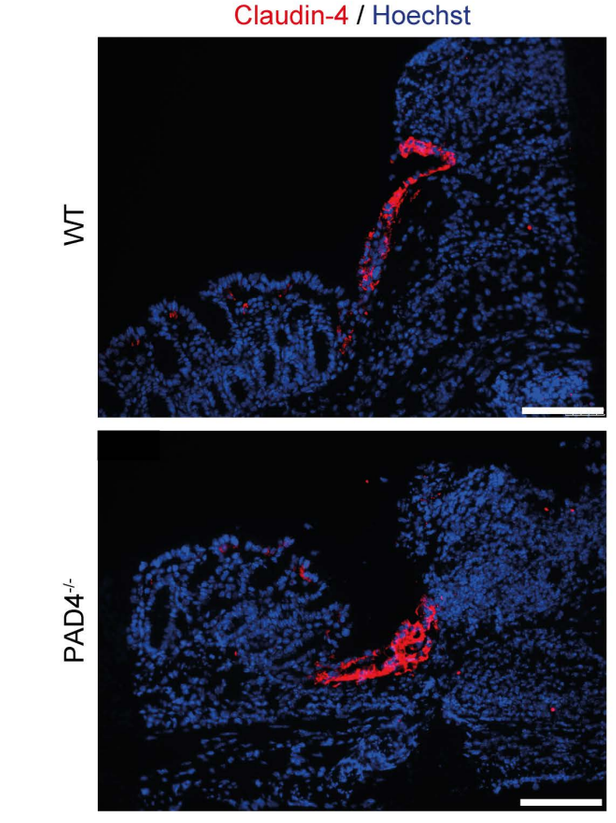
F
Claudin-4 / Hoechst
WT
PAD4-/-

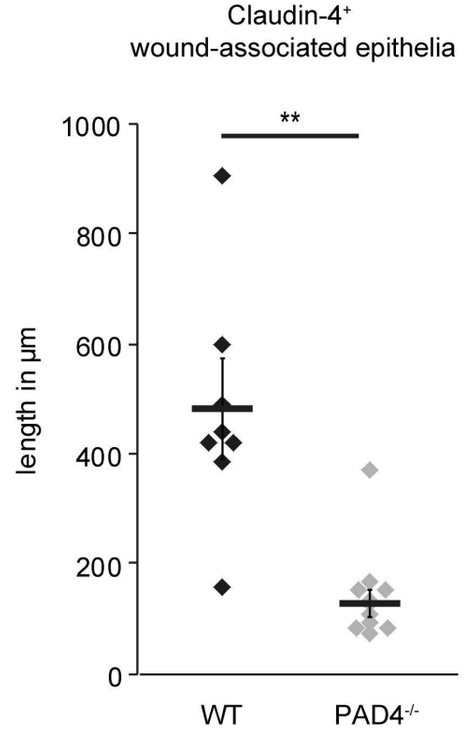
G
Claudin-4+ wound-associated epithelia
**
length in µm
1000
800
600
400
200
0
WT
PAD4-/-

Supplementary Figure 5: Epithelial restitution by wound-associated epithelial cells is improved in the presence of PAD4-dependent immunothrombi

(A) Colon sections of DSS-treated mice were stained by haematoxylin and eosin (H&E) on day 9 after DSS. Here, a completely eroded mucosa was noted in PAD4-/- mice, whereas in WT mice, the mucosa was mildly inflamed with nearly intact crypt architecture. **(B)** The eroded surface of the colon as related to the complete mucosal surface was measured on random cross-sections of the distal colon as in (A). The quantitative analysis supports the increased presence of erosions in $PAD4^{-/-}$ mice. (*** $p < 0.001$, Student's t test) **(C)** β-catenin and E-cadherin staining corroborates the increased proportion of eroded mucosa in $PAD4^{-/-}$ mice. **(D)** Colon sections of DSS-treated mice were stained by haematoxylin and eosin (H&E) as in (A). While less frequent in WT mice, areas of crypt loss were detected in both experimental groups. Please note, that in wild-type mice, adjacent wound-associated epithelia repopulate the area with a lost crypt architecture (black line), whereas this response is disturbed in $PAD4^{-/-}$ mice. (n 20–24 mice per group studied, respectively). **(E)** The fraction of the mucosal surface with lost crypt architecture, which is covered by wound-associated epithelia as in (D) was quantified (*** $p < 0.001$, Student's t test) **(F)** The edge of forceps-induced colon wounds was studied regarding the presence and length of the layer of claudin-4^{+} wound-associated epithelia employing immunofluorescence. Representative images are shown displaying a shorter layer of wound-associated epithelia in $PAD4^{-/-}$ mice. **(G)** The length of the layer of wound-associated epithelia as presented in (E) was quantified (n = 8 samples per group studied) (** $p < 0.01$ Student's t test). Scale bars equal 100 µm throughout the figure.

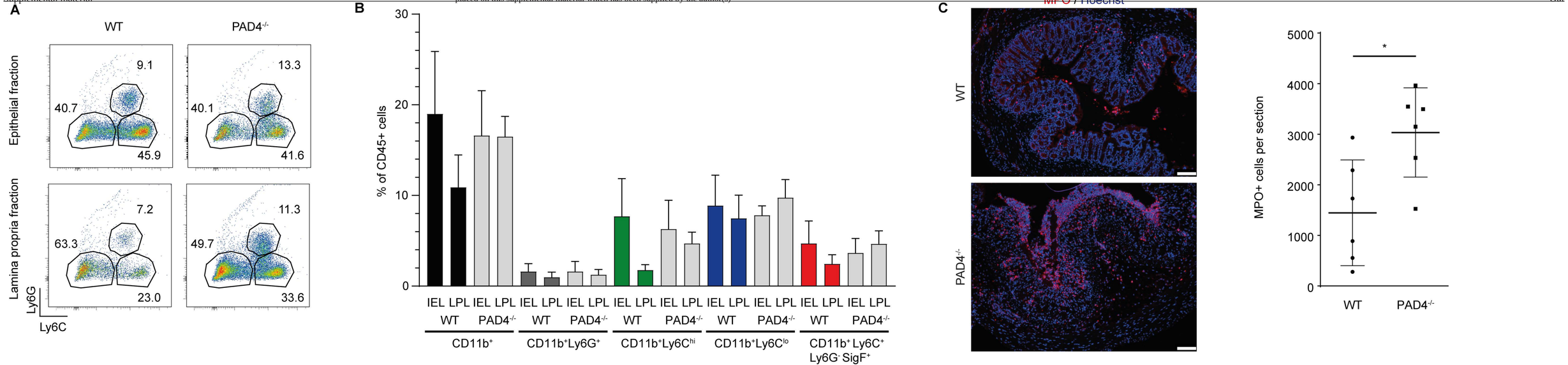

Supplementary Figure 6: Analyses of immune cell populations in colon tissue in the course of DSS-induced colitis in wild-type and PAD4$^{-/-}$ mice

(A, B) Flow cytometric analysis of colon tissue from wild-type and PAD4$^{-/-}$ mice subjected to 3 % DSS in the drinking water for 7 days. Both mouse strains exhibit ample infiltration of various myeloid cell populations to the bowel wall. Both the intraepithelial and lamina propria fraction are depicted (n = 6 samples per group), while luminal leukocytes are not represented in these analyses. **(C)** Immunofluorescence (left) of colon sections of DSS-treated mice show the marked infiltration of MPO^{+} granulocytes to the eroded mucosa in both groups. The eroded area in PAD4$^{-/-}$ mice is covered by a layer of myeloperoxidase (MPO)-positive neutrophils. Quantification (right) of MPO-positive cells in cross-sections of DSS-induced colitis reveals a significantly higher invasion of neutrophils in PAD4$^{-/-}$ mice compared to wild-type, when luminal neutrophils are accounted for (sections of n = 6 mice evaluated).

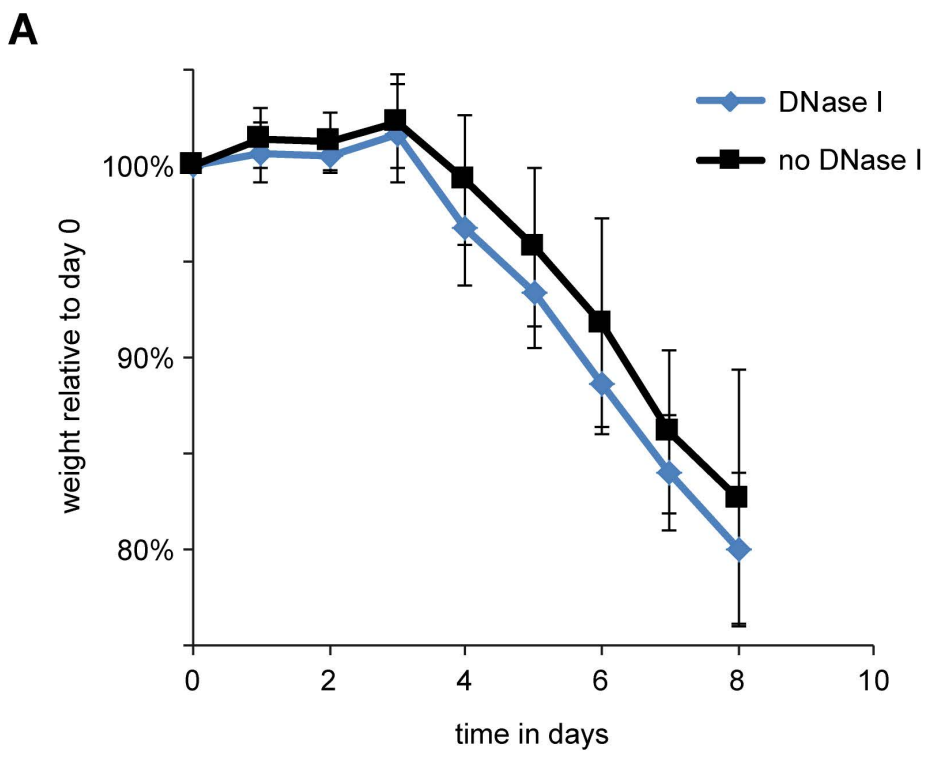
A
DNase I
no DNase I
100%
90%
80%
weight relative to day 0
0
2
4
6
8
10
time in days

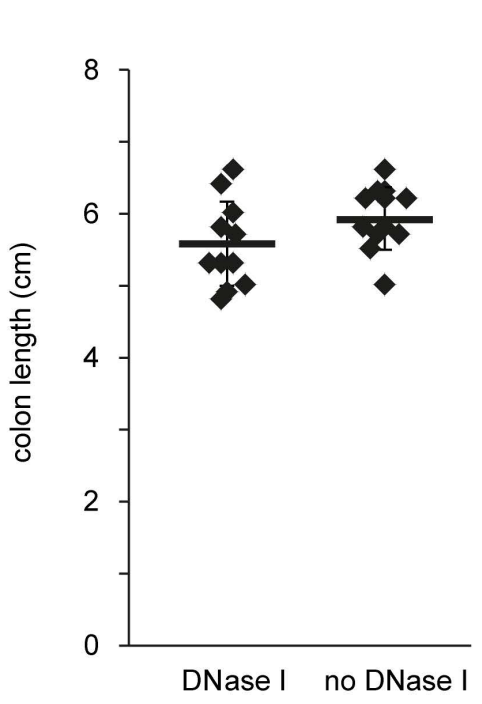
B
8
6
4
2
0
colon length (cm)
DNase I
no DNase I

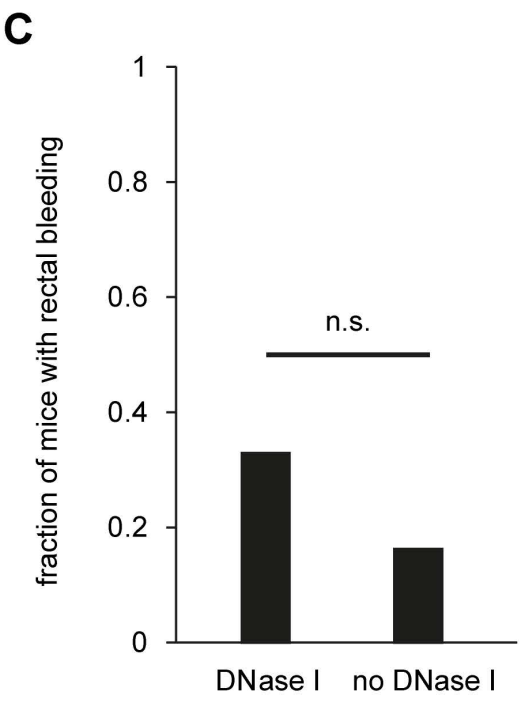
C
1
0.8
0.6
0.4
0.2
0
fraction of mice with rectal bleeding
n.s.
DNase I
no DNase I

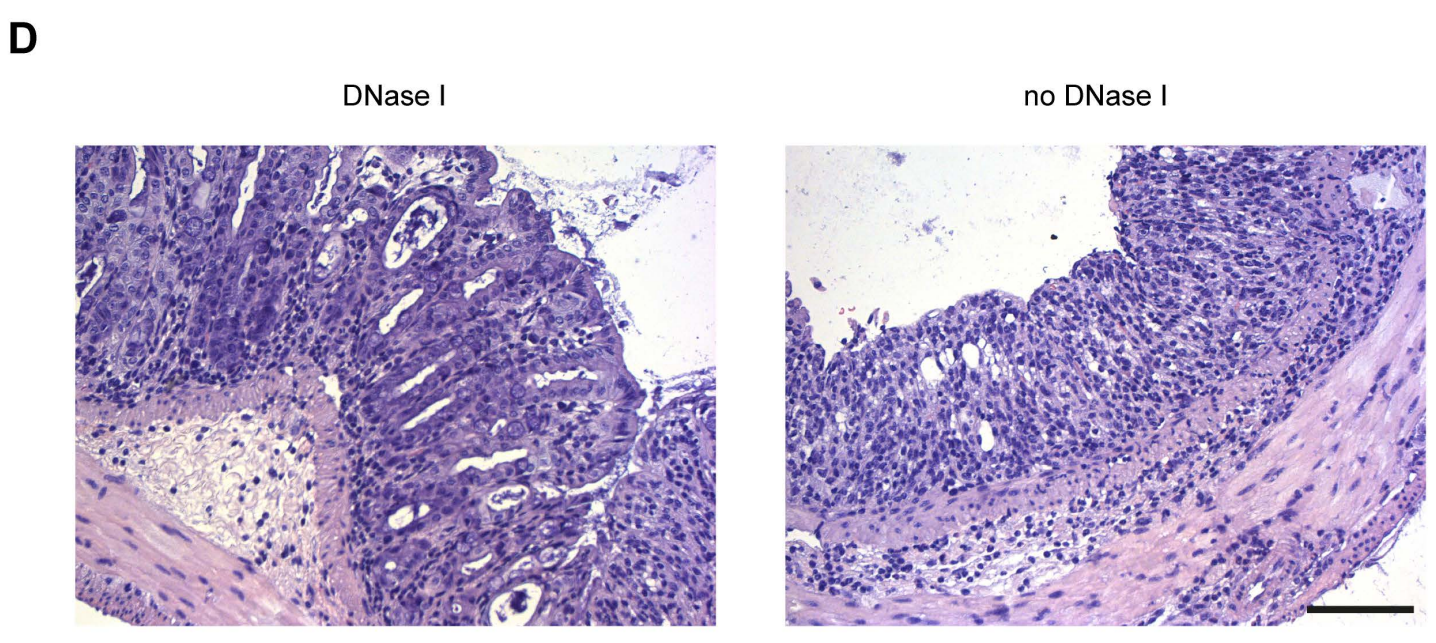
D
DNase I
no DNase I

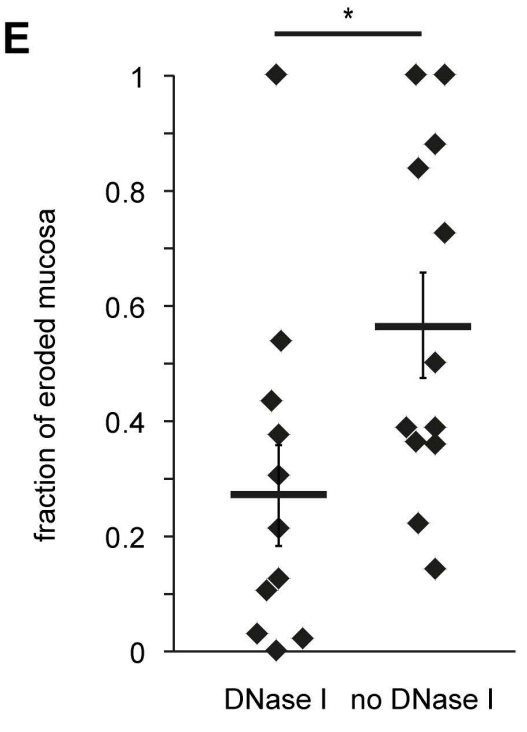
E
*
1
0.8
0.6
0.4
0.2
0
fraction of eroded mucosa
DNase I
no DNase I

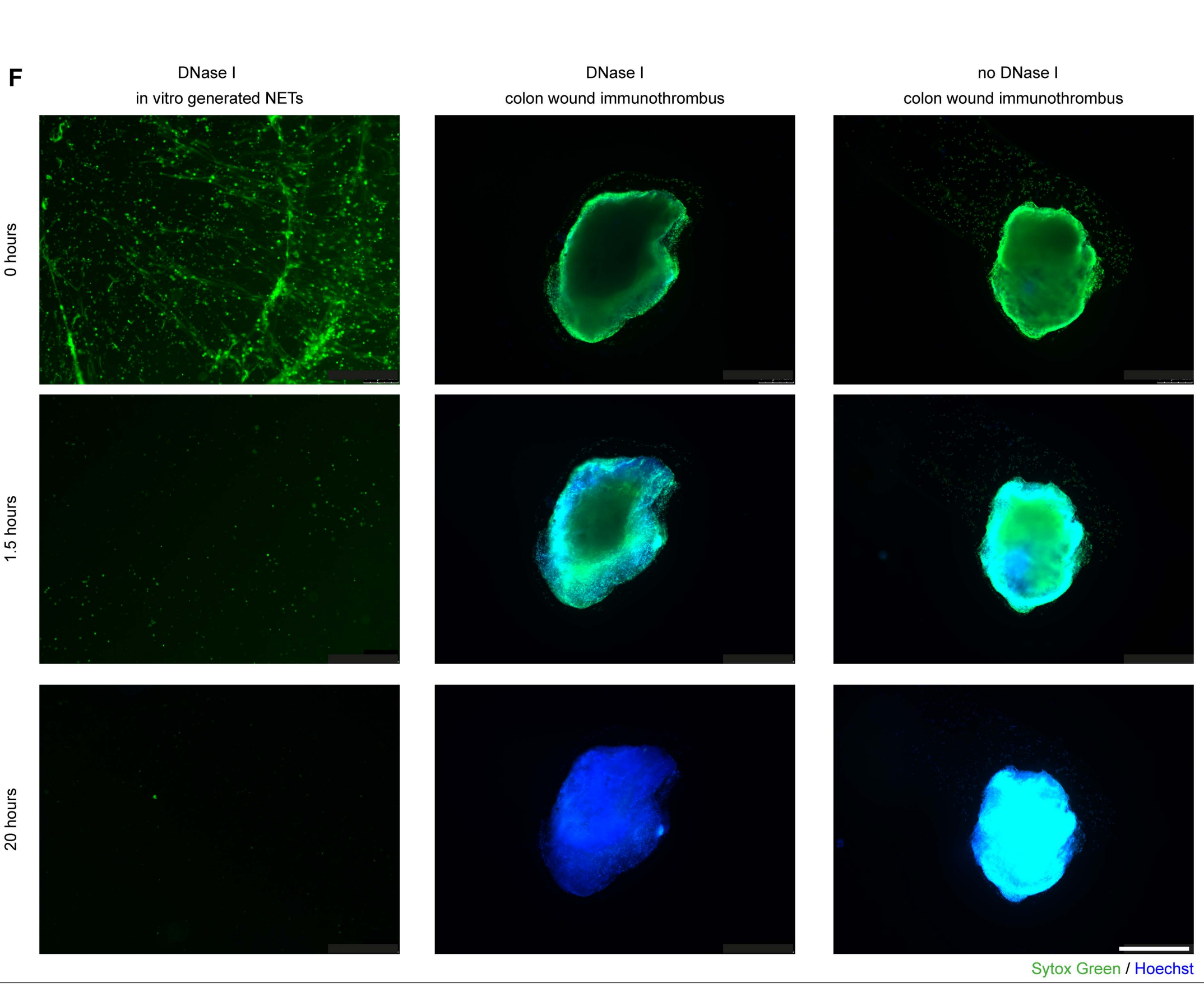
F
DNase I
in vitro generated NETs
DNase I
colon wound immunothrombus
no DNase I
colon wound immunothrombus
0 hours
1.5 hours
20 hours
Sytox Green / Hoechst

Supplementary Figure 7: DNase I does not facilitate rectal bleeding in DSS-induced colitis

Wild-type mice were treated with 3% DSS in drinking water for 7 days and injected intravenously with DNase I (5U/g) or control every day. **(A)** DNase I treatment did not affect weight loss, **(B)** colon length or **(C)** rectal bleeding frequency induced by DSS treatment. **(D)** Histological stainings of colon sections revealed reduced erosions in mice treated with DNase I (scale bar = 100 µm). **(E)** The fraction of eroded mucosa was reduced in DNase-I-treated animals as determined from images as in (D) (* $p < 0.05$, Student's t test, n: 12 mice per group). **(F)** *In-vitro* generated NETs (stimulus: 50mM $NaHCO_3$) can be effectively digested by DNase I (1U/ml). In contrast, ex-vivo colon wound immunothrombi incubated with DNase I (1U/ml) exhibit a markedly slower reduction of intercalating SYTOX Green staining over time and retained major grove-binding Hoechst signal, but are not disintegrated among enzymatic treatment (scale bar = 500 µm, representative of 3 independent experiments).

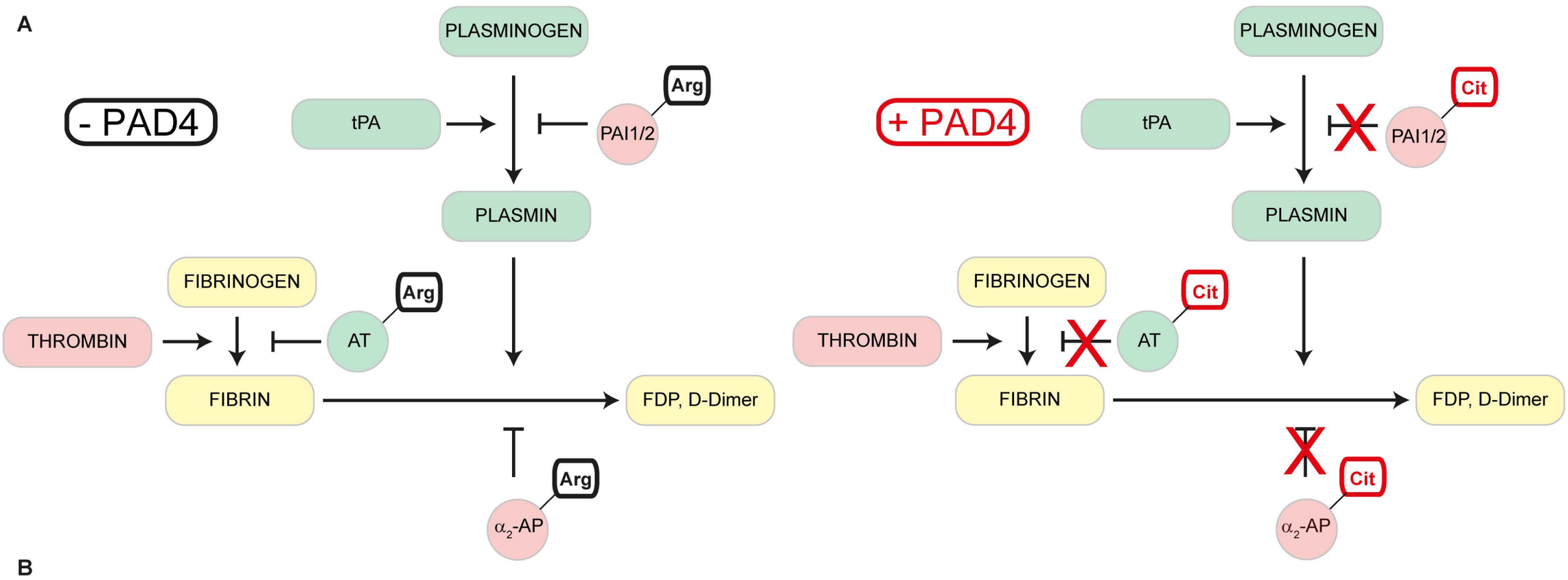
A
PLASMINOGEN
- PAD4
tPA
PAI1/2
Arg
PLASMIN
FIBRINOGEN
THROMBIN
AT
Arg
FIBRIN
FDP, D-Dimer
α2-AP
Arg
+ PAD4
PLASMINOGEN
tPA
PAI1/2
Cit
PLASMIN
FIBRINOGEN
THROMBIN
AT
Cit
FIBRIN
FDP, D-Dimer
α2-AP
Cit

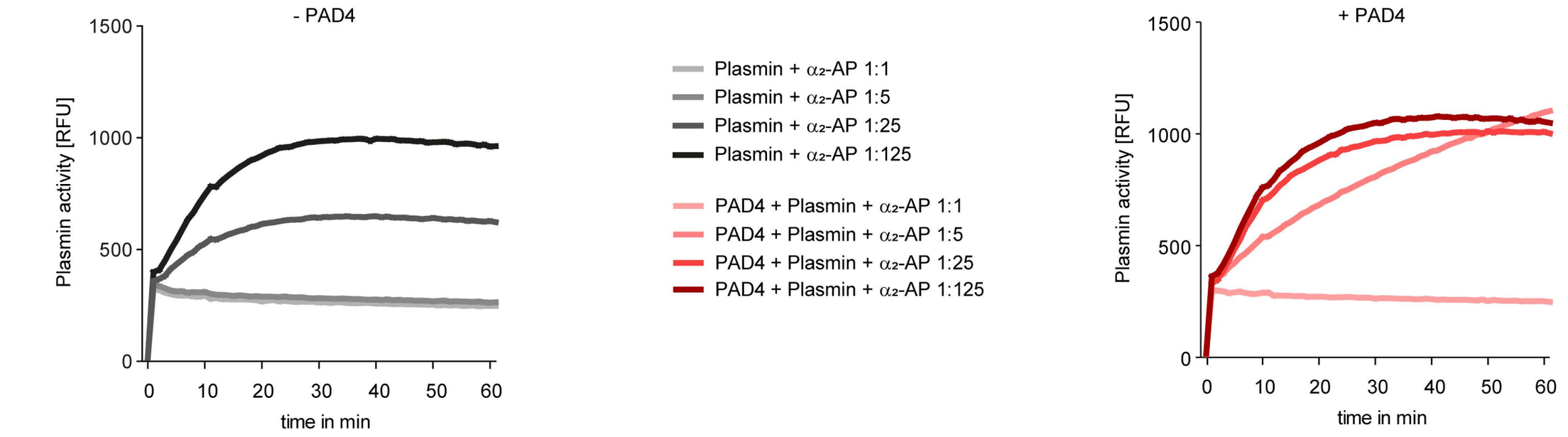
B
- PAD4
Plasmin activity [RFU]
time in min
Plasmin + α2-AP 1:1
Plasmin + α2-AP 1:5
Plasmin + α2-AP 1:25
Plasmin + α2-AP 1:125
PAD4 + Plasmin + α2-AP 1:1
PAD4 + Plasmin + α2-AP 1:5
PAD4 + Plasmin + α2-AP 1:25
PAD4 + Plasmin + α2-AP 1:125
+ PAD4
Plasmin activity [RFU]
time in min

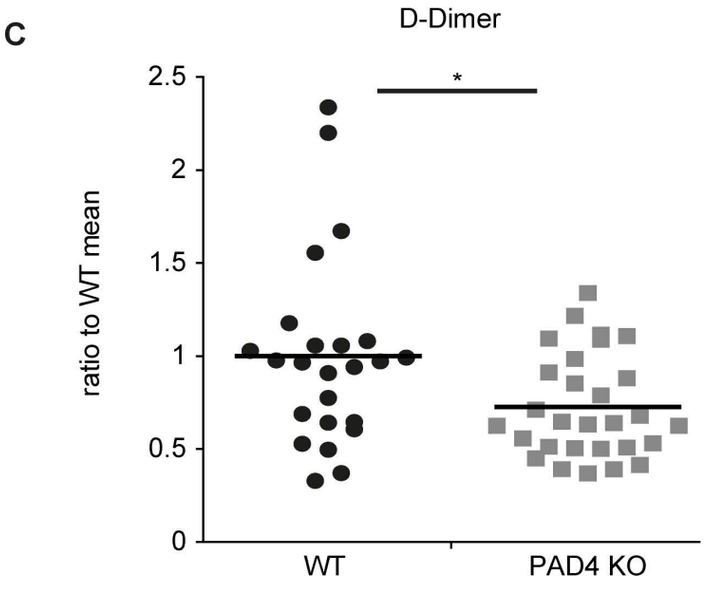
C
D-Dimer
ratio to WT mean
*
WT
PAD4 KO

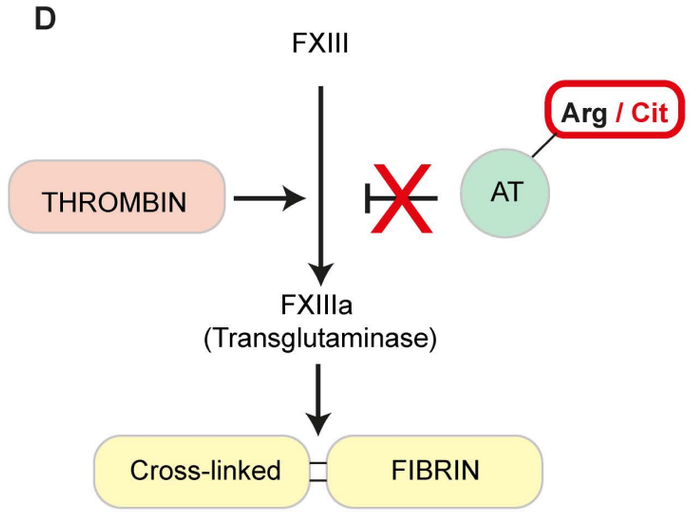
D
FXIII
THROMBIN
AT
Arg / Cit
FXIIIa
(Transglutaminase)
Cross-linked
FIBRIN

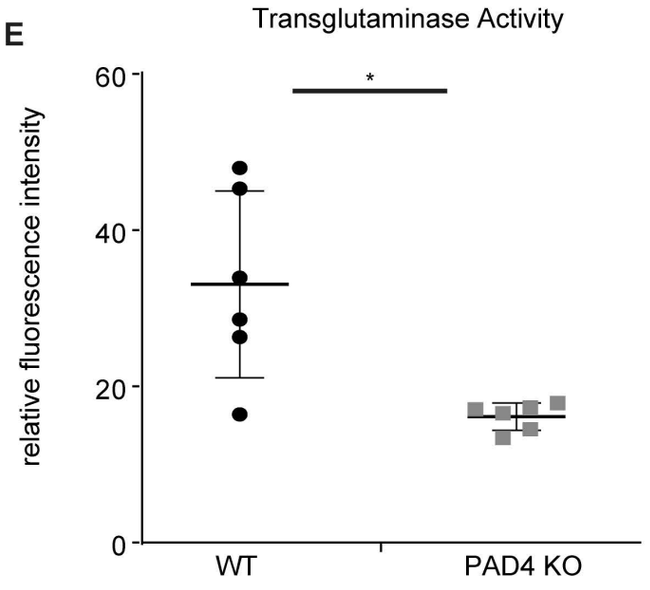
E
Transglutaminase Activity
relative fluorescence intensity
*
WT
PAD4 KO

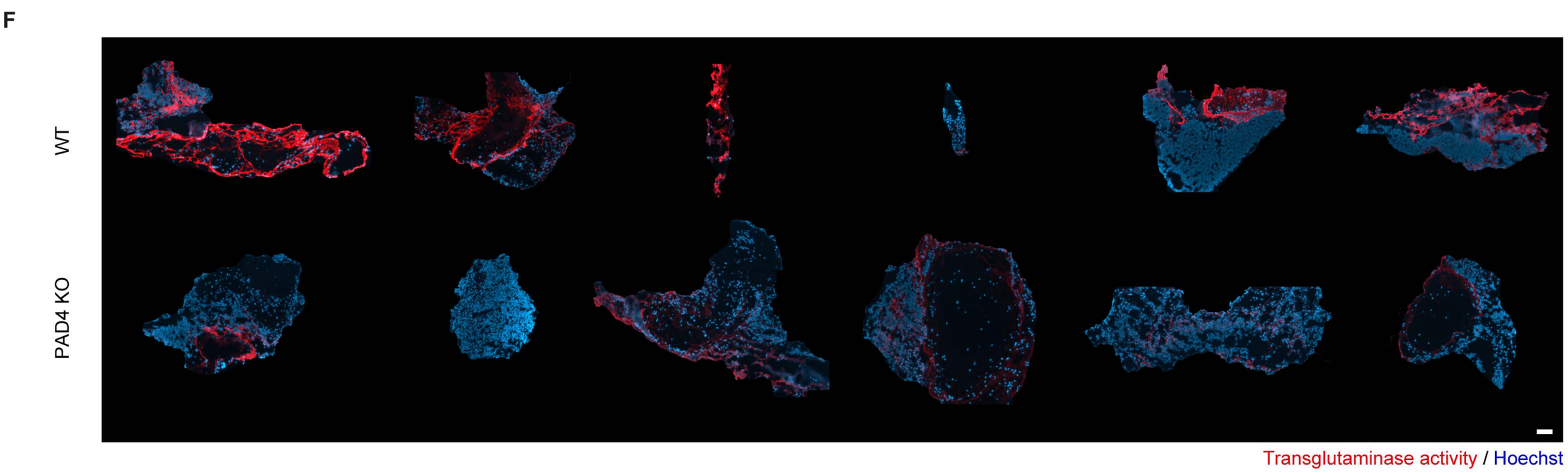
F
WT
PAD4 KO
Transglutaminase activity / Hoechst

Supplementary Figure 8: PAD4 affects the balance between coagulation and fibrinolysis via serpin inactivation and facilitates thrombus remodelling by transglutaminases

(A) A simplified model of the coagulation and fibrinolysis cascade is presented. Serine proteases interact with their respective serine protease inhibitors (serpins), numerous of which carry an arginine in their P1 reactive site (highlighted with Arg). PAD4 can suppress serpin functionality and thus impact the coagulation-fibrinolysis balance on multiple levels (tPA = tissue plasminogen activator; PAI1/2 = plasminogen activator inhibitor-1/2; AT = antithrombin; α_2-AP = α_2-antiplasmin) (modified arginine highlighted with Cit). **(B)** Active plasmin was incubated together with the fluorescent substrate N-Succinyl-Ala-Phe-Lys-AMC and α_2-antiplasmin in various dilutions at 37 °C *in vitro* in the presence or absence of PAD4. Citrullination of α_2-antiplasmin by PAD4 diminished its inhibitory activity on plasmin activity in a dose-dependent manner. One representative experiment of 5 independent experiments is shown. **(C)** D-dimer concentrations were assessed by ELISA in protein extracts of colon wounds from wild-type and PAD4$^{-/-}$ mice harvested 4–48 hours after wounding. A ratio to the wild-type mean of each time point was calculated to correct for differences in concentration over time. (N: 25–29 samples were studied, * $p < 0.05$, Student's t-test) **(D)** A simplified model of fibrin cross-linking by the thrombin-activated transglutaminase FXIIIa is presented. **(E)** Transglutaminase activity was assessed in colon wounds of wild-type and PAD4 knockout mice *in vivo* by i. p. injection of the biotin-labelled substrate biotin-amido-pentylamine (100 mg/kg) before wound induction and subsequent streptavidin-aided fluorescent detection. Relative fluorescence units were measured on tissue sections as in (F), showing significantly increased transglutaminase activity in the wounds of wild-type mice as compared to PAD4$^{-/-}$ mice (N: 6 wounds per group). **(F)** Histochemical detection of transglutaminase activity in sections of wild-type and PAD4$^{-/-}$ colon wounds reveals marked transglutaminase activity restricted to the wound bed. Wild-type wounds display a stronger increase in transglutaminase activity as compared to PAD4$^{-/-}$ samples.